Supporting information

MOF-derived 3D host nanostructures combining the advantages of microporous MOFs and carbon for stable Li deposition

Ju Young Kim[‡a], Jae Hun Choi[‡a], Jung-Kul Lee[*b], and Yun Chan Kang[*a]

[a]Department of Materials Science and Engineering, Korea University, Anam-Dong, Seongbuk-Gu, Seoul 136-713, Republic of Korea.

[b]Department of Chemical Engineering, Konkuk University, Hwayang-dong, Gwangjingu, Seoul 143-701, Republic of Korea.

[‡] These two authors contributed equally to this work.

[*]Corresponding authors.

E-mail addresses: jkrhee@konkuk.ac.kr (J.-K. Lee), yckang@korea.ac.kr (Y.C. Kang)

Experimental Section

Material characterization

The microstructures and morphologies were observed using scanning electron microscopy (SEM; TESCAN, VEGA3) with secondary electron imaging, and transmission electron microscopy (TEM; JEOL, JEM-2100F). The crystal structures were determined by X-ray diffraction (XRD; X'Pert PRO MPD) with Cu Kα radiation (λ= 1.54 Å). The surface chemical states of the samples were analyzed using X-ray photoelectron spectroscopy (XPS; K-Alpha, Thermo Scientific) with an Al Kα X-ray source. The specific surface areas and pore structures of the samples were estimated using N_2 adsorption-desorption measurements based on the Brunauer–Emmett–Teller (BET) method (Belsorp mini II). The vibrational modes of the samples were analyzed using Raman spectroscopy (LabRAM HR Evolution Visible_NIR, HORIBA) with a 632.8 nm He–Ne laser as the excitation source. Four-point probe (AiT, CMT-SR2000N) was used to measure the electrical conductivity of the electrodes at the range of 5 μS cm^{-1} to 100 kS cm^{-1}.

Electrochemical measurement

The electrode was prepared by mixing the sample powder with a polyvinylidene fluoride (PVDF) binder in a 9:1 ratio to create a slurry. After mixing with a proper dosage of N-methyl-2-pyrrolidone (NMP), the homogeneous slurry was applied onto a Cu foil with a thickness of 20 μm using a doctor blade. The resulting slurry was dried in an 80 °C oven overnight, and the mass loading of the electrode was 1.0 mg cm^{-2}. Asymmetric cell tests were performed using CR2032 coin-type half-cells, in which the host electrode (14 mm diameter) served as the working electrode and lithium foil (16 mm diameter) was used as both the counter and reference electrode. All cell assembly procedures were conducted in an Ar-filled glove box (H_2O and O_2 < 1 ppm). A polypropylene film was employed as the separator, and the electrolyte consisted of 1 M lithium bis(trifluoromethanesulfonyl)imide (LiTFSI) and 0.3 M $LiNO_3$ dissolved in a 1:1 volumetric mixture of 1,3-dioxolane (DOL) and 1,2-dimethoxyethane (DME). To stabilize the solid electrolyte interphase (SEI) and eliminate surface impurities, the cells were initially precycled for two cycles in the voltage range of 0–1.0 V at a current density of 1.0 mA cm^{-2}. Following SEI stabilization, lithium plating and stripping were performed under various conditions, with current densities of 1.0, 2.0, and 5.0 mA cm^{-2} and areal capacities of 1.0 and 2.0 mAh cm^{-2}. In each cycle, lithium was deposited at a controlled areal capacity, followed by stripping to 1.0 V. The Coulombic

efficiency (CE), defined as the ratio of stripped to deposited capacity, was monitored during repeated plating/stripping cycles until a sharp decline in CE marked the end of the test.

Symmetric cell tests were conducted using CR2032 coin-type cells. Prior to assembly, lithium was deposited onto the host electrodes by applying a current density of 2.0 mA cm^{-2} for 2.5 hours, corresponding to a total areal capacity of 5.0 mAh cm^{-2}. The deposition process was carried out using half-cells prepared in the same manner as for asymmetric cell tests. Two identical Li-preloaded electrodes obtained from separate half-cells were disassembled and reassembled into a symmetric configuration. As both electrodes were pre-loaded with lithium and electrochemically identical, the initial open-circuit voltage (OCV) of the symmetric cell was approximately 0 V. During each cycle, one electrode underwent lithium stripping while the other underwent lithium plating. The current direction was then reversed to alternate the roles of the electrodes. This charge–discharge alternation was repeated continuously until either a short circuit occurred or the cell exhibited a sharp increase in overpotential, indicating failure. The $LiNi_{0.8}Co_{0.1}Mn_{0.1}O_2$ (NCM811) cathode was prepared by mixing NCM811, Super-P, and PVDF at a ratio of 8:1:1 to create a slurry, which was then pasted onto an Al foil. The mass loading of the NCM811 cathode was 6.1 mg cm^{-2}. The electrolyte used for the full-cell tests was 1 M LiPF6 in ethylene carbonate (EC) and ethyl methyl carbonate (EMC) (3:7 v/v) with 2 wt% fluoroethylene carbonate (FEC), and the voltage range was 2.5–4.2 V. With a theoretical capacity of 200 mAh g^{-1} for NCM811, the resulting N/P ratio of the full cell was calculated to be 4.2. The $LiFePO_4$ (LFP) cathode was prepared with an areal mass loading of 5.69 mg cm^{-2}, corresponding to a theoretical capacity of approximately 0.94 mAh cm^{-2} based on the standard specific capacity of 165 mAh g^{-1}. The ZIF-C500 anode was pre-loaded with 5.0 mAh cm^{-2} of Li using the same protocol as for symmetric cells, resulting in a calculated N/P ratio of 5.3.

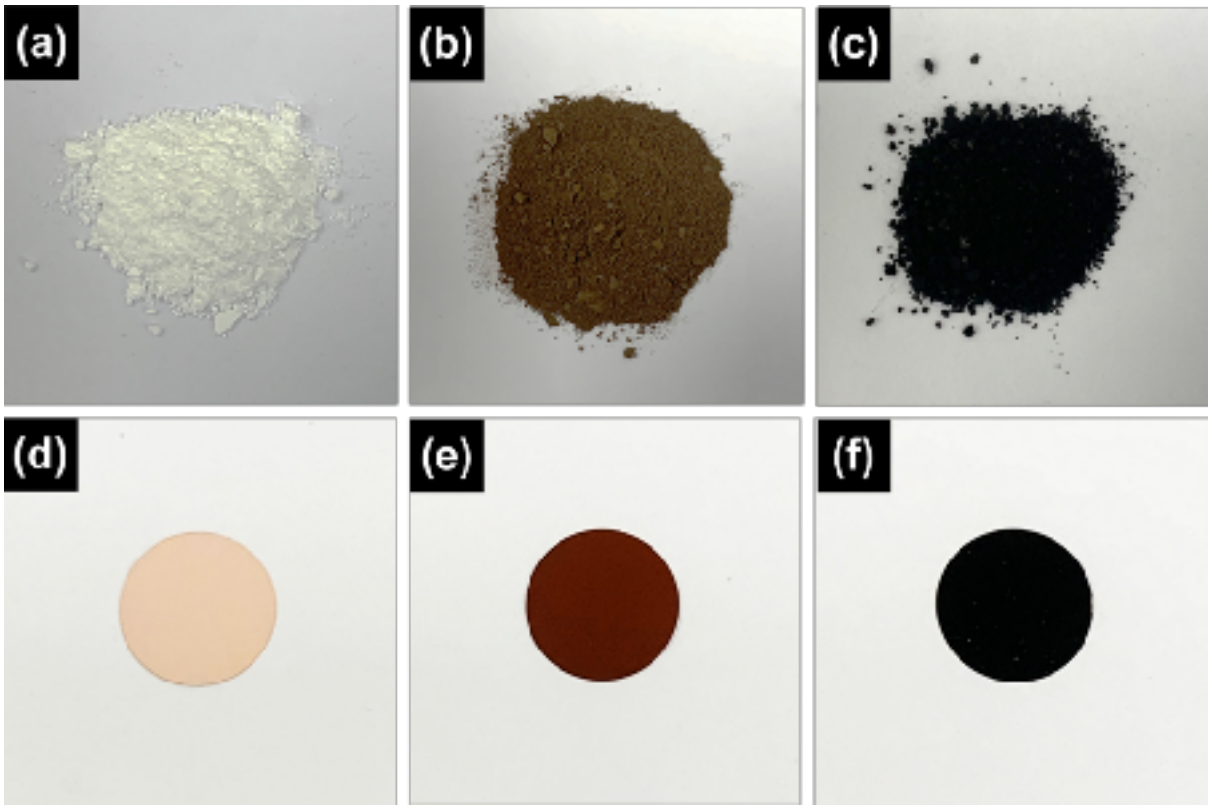

Fig. S1. Photos of (a) ZIF-bare, (b) ZIF-C500, and (c) ZIF-C800 powders, and (d) ZIF-bare, (e) ZIF-C500, and (f) ZIF-C800 electrodes pasted on Cu foil.

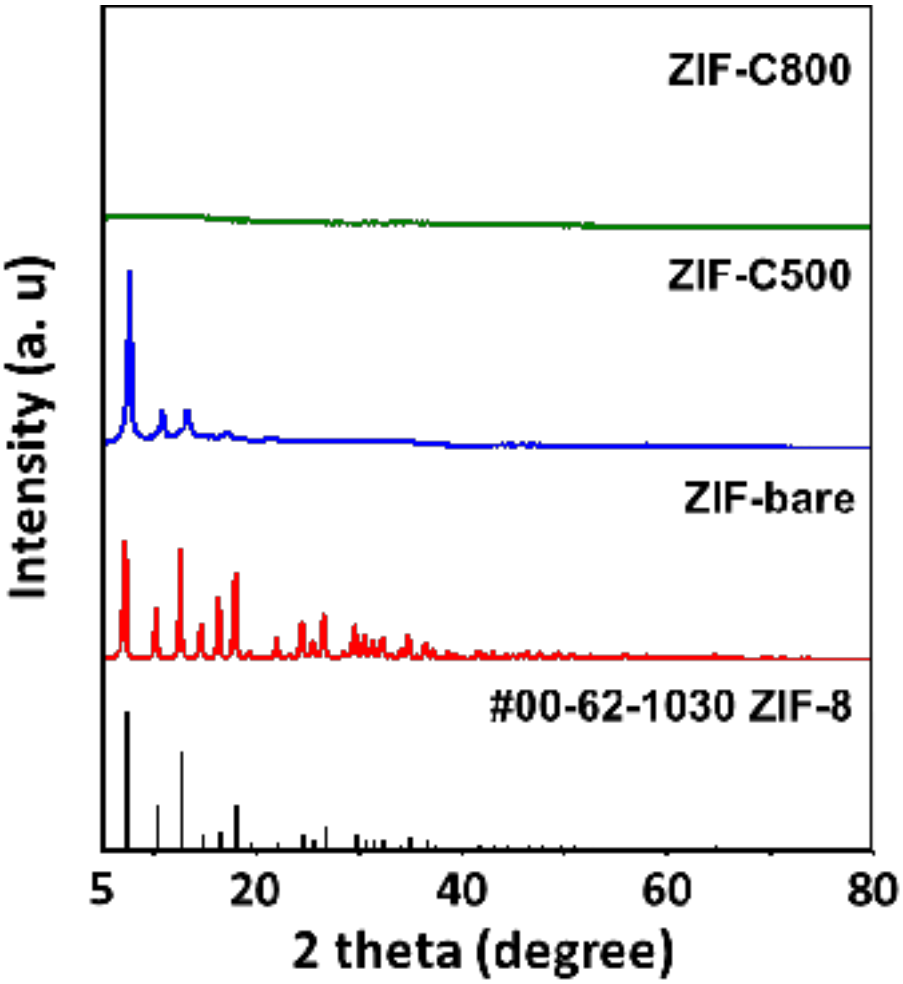

Fig. S2. XRD patterns of ZIF-bare, -C500, and -C800 powders.

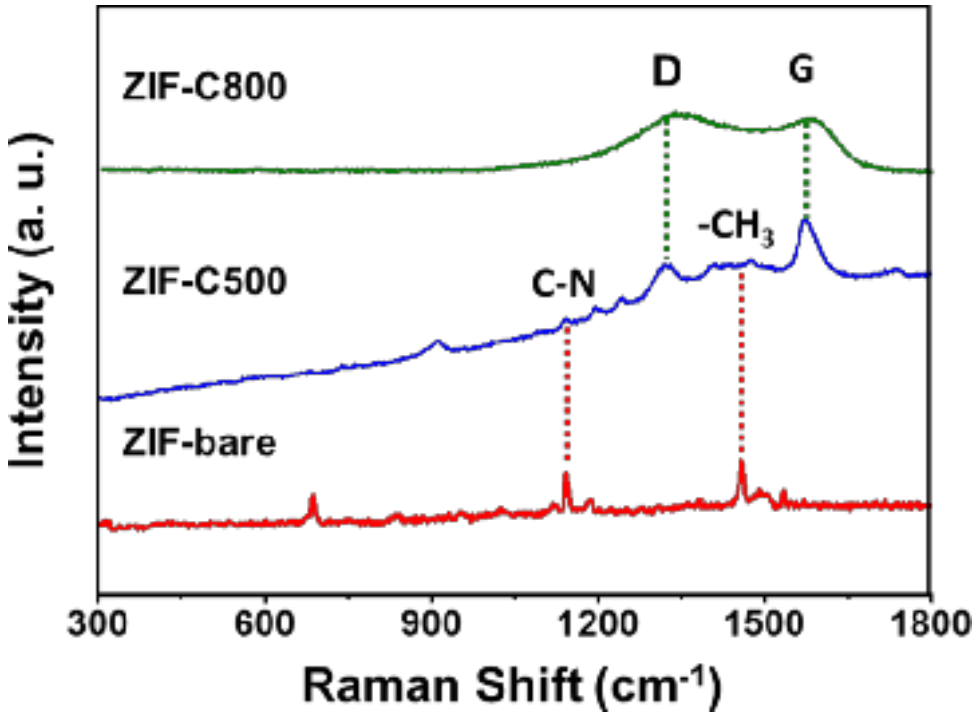

Fig. S3. Raman spectra of ZIF-bare, -C500, and -C800 powders.

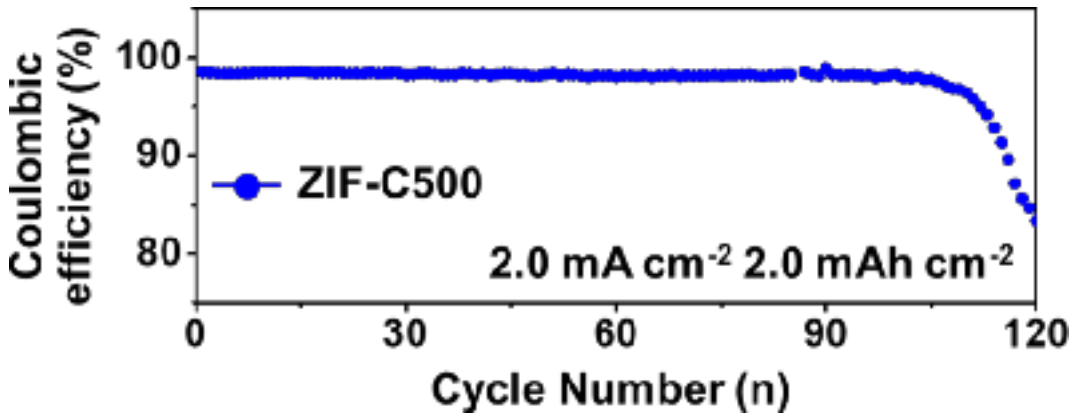

Fig. S4. Coulombic efficiencies of ZIF-C500 obtained from asymmetric cell test cycled at a current density of 2.0 mA cm^{-2} with a capacity of 2.0 mAh cm^{-2}.

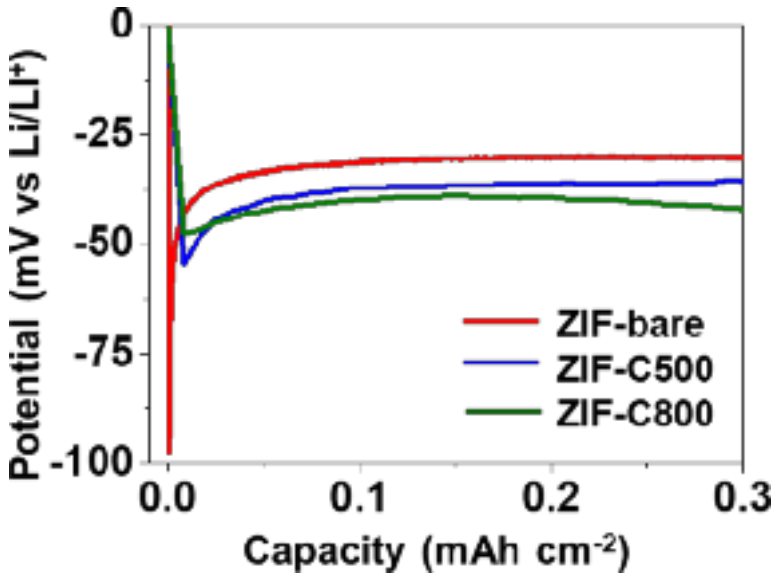

Fig. S5. Enlarged voltage profiles of ZIF-bare, -C500, and -C800 for the purpose of comparing the nucleation overpotentials during lithium deposition.

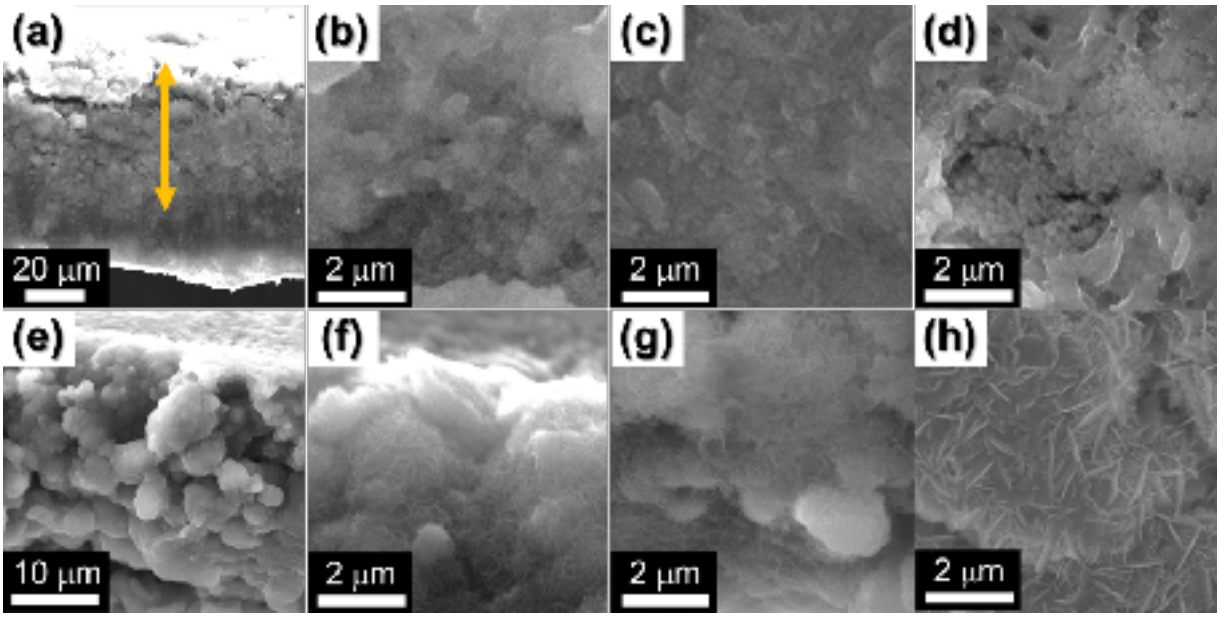

Fig. S6. SEM images of (a-d) ZIF-bare and (e-h) ZIF-C800 after the deposition of 5.0 mAh cm^{-2} of Li: (a and e) Cross-sectional image, (b and f) Upper part of the cross-section, (c and g) Lower part of the cross-section, and (d and h) Top view of the electrodes.

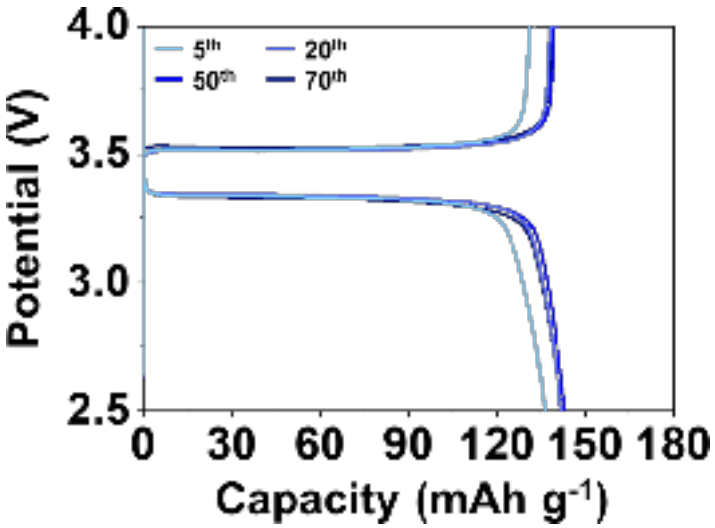

Fig. S7. Voltage profiles for the 5th, 20th, 50th, and 70th cycles, organized based on the results from Fig. 6d, obtained at a current density of 2.0 C.

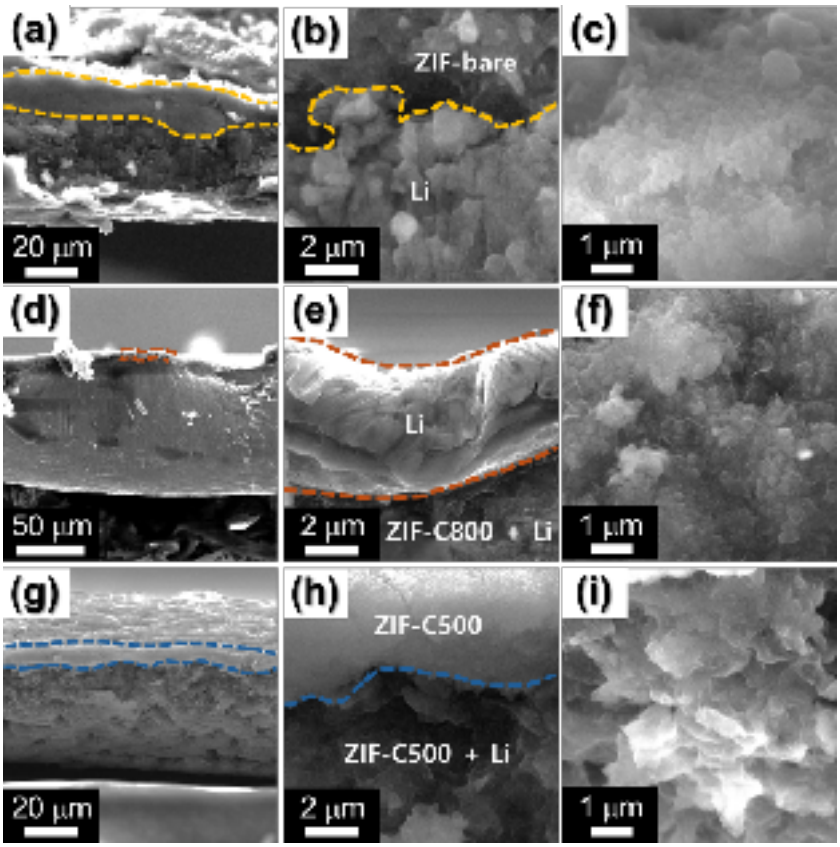

Fig. S8. Cross-sectional SEM images of (a-c) ZIF-bare, (d-f) ZIF-C800, and (g-i) ZIF-C500 electrodes after 100 cycles in asymmetric cells cycled at the current density of 2.0 mA cm^{-2} and the cycling capacity of 1.0 mAh cm^{-2}, and magnified images of (b and c) ZIF-bare, (e and f) ZIF-C800, and (h and i) ZIF-C500 electrodes.

Table S1. Performance comparison of asymmetric cell tests.

Samples	Calcination conditions	Capacity	Current density	Cycle	Coulombic efficiency	Nucleation overpotential	Ref
ZIF-C500	**500 °C 2 h**	**1.0 mAh cm^{-2}**	**1.0 mA cm^{-2}**	**220 cycles**	**98.0 %**	**18.2 mV (@ 2 mA cm^{-2})**	**This work**
		1.0 mAh cm^{-2}	**2.0 mA cm^{-2}**	**150 cycles**	**98.1 %**		
		1.0 mAh cm^{-2}	**5.0 mA cm^{-2}**	**100 cycles**	**96.5 %**		
		2.0 mAh cm^{-2}	**2.0 mA cm^{-2}**	**100 cycles**	**98.5 %**		
MIL-125(Ti)-MOF	-	1.0 mAh cm^{-2}	0.5 mA cm^{-2}	400 cycles	98.0 %	51.0 mV (@ 0.5 mA cm^{-2})	[S1]
		1.0 mAh cm^{-2}	1.0 mA cm^{-2}	100 cycles	90.0 %		
Cu-MOFs	-	1.0 mAh cm^{-2}	2.0 mA cm^{-2}	180 cycles	98.4 %	-	[S2]
		1.0 mAh cm^{-2}	3.0 mA cm^{-2}	120 cycles	84.1 %		
		1.0 mAh cm^{-2}	5.0 mA cm^{-2}	120 cycles	72.5 %		
Al-PCRs/CNTs	900 °C 5 h	1.0 mAh cm^{-2}	0.5 mA cm^{-2}	300 cycles	98.7 %	-	[S3]
ZGIL	800 °C 2 h / -	1.0 mAh cm^{-2}	1.0 mA cm^{-2}	300 cycles	97.6 %	28.0 mV (@ 1 mA cm^{-2})	[S4]
ICDL	700 °C 3 h / -	1.0 mAh cm^{-2}	1.0 mA cm^{-2}	220 cycles	96.6 %	35.0 mV (@ 0.5 mA cm^{-2})	[S5]
		2.0 mAh cm^{-2}	1.0 mA cm^{-2}	200 cycles	93.5 %	81.0 mV (@ 1 mA cm^{-2})	
		1.0 mAh cm^{-2}	3.0 mA cm^{-2}	110 cycles	93.6 %	92.0 mV (@ 3 mA cm^{-2})	

S1. W. Xu, J. Cao, P. Jia, C. Tao, X. Wang, L. Wang, and T. Liu, *ACS Appl Mater Interfaces*, 2023, **15**, 51281-51288.

S2. Z. Jiang, T. Liu, L. Yan, J. Liu, F. Dong, M. Ling, C. Liang, and Z. Lin, *Energy Storage Mater*, 2018, **11**, 267-273.

S3. M. Ali, T. Zhao, S. Iqbal, W. Zhao, H. Wang, S. Liu, S. Li, Z. Wang, and Y. Ma, *Chem Eng J*, 2022, **431**, 134194.

S4. Y. Shi, S. Yang, X. Sun, G. Ai, T. Zhang, F. Wu, and W. Mao, *Electrochim Acta*, 2022, **417**, 140333.

S5. J. Man, W. Liu, H. Zhang, K. Liu, Y. Cui, J. Yin, X. Wang, and J. Sun, *J Mater Chem A*, 2021, **9**, 13661.